



UNIVERSIDADE ESTADUAL DE CAMPINAS
SISTEMA DE BIBLIOTECAS DA UNICAMP
REPOSITÓRIO DA PRODUÇÃO CIENTÍFICA E INTELLECTUAL DA UNICAMP

Versão do arquivo anexado / Version of attached file:

Versão do Editor / Published Version

Mais informações no site da editora / Further information on publisher's website:

<https://link.springer.com/article/10.1007%2Fs11356-019-04215-0>

DOI: 10.1007/s11356-019-04215-0

Direitos autorais / Publisher's copyright statement:

©2019 by Springer. All rights reserved.

DIRETORIA DE TRATAMENTO DA INFORMAÇÃO

Cidade Universitária Zeferino Vaz Barão Geraldo

CEP 13083-970 – Campinas SP

Fone: (19) 3521-6493

<http://www.repositorio.unicamp.br>



H₃PO₄-activated carbons produced from açai stones and Brazil nut shells: removal of basic blue 26 dye from aqueous solutions by adsorption

Thielle Nayara Vieira de Souza¹ · Melissa Gurgel Adeodato Vieira² · Meuris Gurgel Carlos da Silva² · Davi do Socorro Barros Brasil¹ · Samira Maria Leão de Carvalho¹

Received: 26 July 2018 / Accepted: 9 January 2019 / Published online: 30 January 2019
© Springer-Verlag GmbH Germany, part of Springer Nature 2019

Abstract

The adsorption characteristics of C.I. basic blue 26 (BB26) from aqueous solutions onto H₃PO₄-activated carbons (ACs) produced from açai stones (*Euterpe oleracea* Martius) and Brazil nut shells (*Bertholletia excelsa* H. B. K) were investigated in a batch system. The ACs were characterized by XRD, FT-IR, N₂ adsorption at 77 K, mercury porosimetry, and acidity/basicity analysis. The pseudo-first-order, pseudo-second-order kinetic models and intraparticle diffusion model were used for the kinetic interpretations. The adsorption processes follow the pseudo-second-order kinetic model. The Boyd plots revealed that the adsorption processes were mainly controlled by film diffusion. Equilibrium data were analyzed by the Langmuir and Freundlich models, at different temperatures. The equilibrium data were best represented by the Langmuir isotherm. The adsorption processes were found to be favorable, exothermic, and spontaneous. The açai stones and Brazil nut shells-based ACs were shown to be effective adsorbents for removal of BB26 from aqueous solutions.

Keywords Adsorption · Activated carbon · Chemical activation · Basic blue 26 · Brazil nut shell · Açai stone

Introduction

The synthetic dyes are in a class of important environmental pollutant, since they contaminate large volumes of industrial wastewater and the water resource. The wastewater from textile, pulp and paper, paint, tannery, and dye factories contains significant quantities of these compounds (Crini 2006; Crini and Badot 2008; Gupta and Suhas 2009). A trace quantity of dye present in the water may produce color in the bulk and make it unusable (Kumar et al. 2013). These substances are resistant to the conventional biological treatment methods and are chemically stable to oxidizing agents, light, and heat (Rai et al. 2005). The dyes used in the textile industry have

considerable structural diversity, and are classified in several ways, according to their chemical structure, their application to the types of textile fibers, exposure to light, and others. Synthetic dyes based on applications include various dye groups such as acid dyes, reactive dyes, basic dyes, direct dyes, vat dyes, and disperse dyes. The term “basic dye” is conveniently used to distinguish an application class of textile dyes, which are used to dye synthetic fibers (Demirbas 2009). The basic dye, C.I. basic blue 26 (Victoria Blue B) is a member of the triphenylmethane class; this dye has positively charged groups, and it is widely used for dyeing substrates (anionic), as like nylon, acrylics, wool, and silk. It is also used for staining specimens in bacteriological and histopathological processes (Anirudhan et al. 2014; Kumar and Tamilarasan 2014). The triphenylmethane dyes are characterized by the presence of chromogen containing the phenyl groups bound by the central carbon atom (Forgacs et al. 2004; Przystaś et al. 2012). Although the basic dyes have significant applications, these dyes can cause serious hazards to the water stream and environment due to their synthetic origin and the complex molecular structures. Thus, researchers have dedicated considerable attention to the removal of basic dyes from aqueous medium such as adsorption of basic blue 26 (BB26) by Fly

Responsible editor: Tito Roberto Cadaval Jr

✉ Samira Maria Leão de Carvalho
sleao@ufpa.br

¹ School of Chemical Engineering, Federal University of Pará, Augusto Corrêa Street, 01, Belém, PA 66075-110, Brazil

² School of Chemical Engineering, University of Campinas, Albert Einstein Avenue, 500, Campinas, SP 13083-970, Brazil

ash (Khare et al. 1987), carbon/Zn/alginate polymer composite beads (Kumar and Tamilarasan 2013), carbon/Ba/alginate beads (Kumar et al. 2013), iron-doped titania/silane (Anirudhan et al. 2014), *Prosopis juliflora* bark carbon (Kumar and Tamilarasan 2014), adsorption of rhodamine B and methylene blue (Gupta et al. 2000), basic red 29 (Geetha and Palanisamy 2016), and malachite green (Nethaji et al. 2010).

A number of treatment technologies are available with varying degrees of success to remove synthetic dye from aqueous solution. Some of these processes include coagulation-flocculation (Saitoh et al. 2014), adsorption (Weber et al. 2014), advanced oxidative processes, ion exchange (Wu et al. 2008), and biological treatment (Rodrigues et al. 2014). The adsorption on the AC is considered an efficient and versatile alternative to remove organic pollutants from wastewater (Gupta and Saleh 2013). High specific surface area, large pore structure availability, pore volume, adsorption capacity, chemical surface, and effective regeneration are useful characteristics of activated carbon. Despite its extensive use to treat wastewater, the adsorption by AC is still an expensive process due to high production cost of these adsorbents. This limitation has indeed instigated a growing interest in the production of low-cost activated carbons, especially from agro-industrial wastes and other low-cost raw materials that are abundant worldwide (Aygun et al. 2003; Deng et al. 2009; Gupta and Suhas 2009; Haimour and Emeish 2006; Liou 2010; Prauchner and Rodríguez-Reinoso 2012; Gupta and Saleh 2013; Demiral and Gungor 2016; Tran et al. 2017; Moura et al. 2018; Mo et al. 2018; Souza et al. 2018), to make more attractive the manufacturing process cost of AC. According to Ruthven (1984), for an adsorption process to be developed on a commercial scale requires the availability of a suitable adsorbent in large quantities at economic cost.

The palm *Euterpe oleracea* Martius, commonly known as açai (palm berries), is purple when mature. The açai pulp presents a wide range of health-promoting and therapeutic benefits due to its reportedly elevated levels of antioxidants. Brazil nut tree (*Bertholletia excelsa* H. B. K.) grows in a vast zone of South America, mostly in the region of Pará (Brazil), and is also found in others Amazonian States of Brazil, Peru, Colombia, Venezuela and Ecuador. The fruits are collected from the natural forest, and they have high content of proteins, carbohydrates, unsaturated lipids, vitamins, and essential minerals, also are micronutrient sources, especially selenium, phytosterols, tocopherols, squalene, and phenolic compounds. Açai and Brazil nut trees are of great economic, social, and cultural importance for the Brazilian Amazon region. The açai fruits are almost round, with a diameter varying between 1 and 2 cm, and they are used as a raw material to produce pulp or juice. Most of the açai pulp is consumed regionally, but the açai market has grown as a result of current tendencies:

convenience, regionalism (typical products), natural food (organic), cosmetic products, and functionality. However, the processing of the açai fruits produces a large amount of waste. It is estimated around 400 tons per day of organic wastes. Currently, this waste is disposed of by inappropriate methods in places such as near rivers, street, and uncontrolled landfills. The fruit of the Brazil nut tree is a large spherical woody capsule or pod. Inside each fruit is 12 to 24 nuts or seeds. Brazil nut consists of a hard, thin outer shell and white kernel (edible part of the seed) (Bonelli et al. 2001). Presently, thousands of tons of Brazil nuts (kernel) are exported, and a large waste amount is generated from shelling the nuts. Pará state (Northern Brazil) produced approximately 14,000 tons per year of nuts (kernel), on the average 19,600 tons per year of nut shells. Presently, these solid wastes are used as a fuel.

High availability and low-cost of the precursors (Brazil nut shells and açai stones), production in large scale, and desirable characteristics for application in adsorption (pore size distributions, specific surface area, and functional surface groups) are relevant aspects regarding the utilization of solid wastes, as alternative raw materials to produce ACs, whose benefits will be to reduce the ambient pollution levels, as also to produce a very useful material.

In the present study, activated carbons (ACs) produced from açai fruit stones and Brazil nut shells were investigated with respect to the adsorption mechanisms of C.I. basic blue 26 (BB26) from aqueous solutions. The ACs were prepared by chemical activation with H_3PO_4 , and their physicochemical and textural properties were determined. In addition, the effects of the initial dye concentrations were investigated, and the equilibrium and kinetic data of the adsorption processes were then analyzed to study the adsorption characteristics and mechanisms of BB26 onto ACs. This research is a contribution to the studies on the removal of dyes from the aqueous medium by using activated carbons prepared from low-cost raw materials, and it represents a low-cost environmental solution due to increased added value of the solids wastes.

Material and methods

Preparation of the basic blue 26 solutions

The basic blue 26 dye (BB26), C.I 44045, was used in this study, whose chemical structure is shown in Fig. 1, and it presents characteristics, such as molecular formula $C_{33}H_{32}ClN_3$; molecular mass $506.08 \text{ g mol}^{-1}$, acid dissociation constant pK_a 8.3, and wavelength λ 618 nm. The BB26 dye was purchased from a Brazilian company (this company supplies products for the textile segment), and it was used without purification. Stock solution of BB26 was prepared by dissolving 500 mg of dye in 1 L distilled water

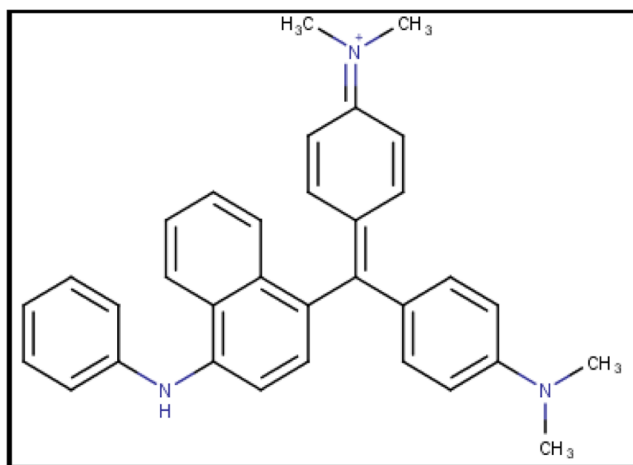


Fig. 1 Chemical structure of the BB26 dye

(0.988 mmol L⁻¹). In the beaker (2 L), the stock solution was stirred at 60 rpm (magnetic stirrer) for 30 min. The test solutions with initial concentrations (0.099–0.790 mmol L⁻¹) were prepared by diluting the stock solution. All dye solutions were prepared immediately before use, and exposure to light was minimized.

Production of activated carbon

The raw materials, açai stone (R1) and Brazil nut shell (R2), were thoroughly cleaned to remove extraneous materials, dried, and ground to smaller particle sizes. In glass tubes (borosilicate), 5 g of the raw material and 10 mL of H₃PO₄ solution (55% by weight) were mixed, and then the glass tubes were placed in a heating system with open reflux at 80 °C for 4 h. The samples were put in crucibles and placed in a muffle furnace set at 450 °C for 2 h. After cooling to room temperature, the resulting carbons were washed several times with hot distilled water (60 °C) until the leachate reached a value of pH between 6.0 and 7.0. The activated carbons (ACs) were dried in an oven at 105 °C for 24 h. The dry samples were crushed and sieved using 12 and 14 mesh sieves and, then these were named AC-R1 (açai stone) and AC-R2 (Brazil nut shell).

Characterization of the AC samples

Physicochemical properties

The total ash content was determined using crucibles containing dried AC heated in a muffle furnace at 650 °C for 6 h based on the procedure by ASTM D2866-11. After heating, the crucibles were allowed to cool in a desiccator, weighed, and then the residue weighed was calculated and reported as percentage of ash. The moisture content of each sample was determined using a standard method (ASTM D2867-17). The AC sample was weighed and dried on oven-drying at 150 °C

for 3 h. The ratio of change in original weight expressed in percentage gives the moisture content.

X-ray diffraction (XRD) measurements were carried out using a PANalytical X'Pert Pro Multipurpose Diffractometer (Philips Analytical Inc.) with copper tube (CuK α , $\lambda = 1.54056 \text{ \AA}$) at 40 Kv and 40 mA. The FT-IR spectra of the samples were recorded by a Nicolet 6700 FT-IR Spectrometer (Thermo Scientific Inc.) using the KBr method at room temperature over a frequency range of 4000–400 cm⁻¹.

Acid-base characteristics

The acidic groups and basic sites on the surfaces of the AC samples were determined, according to the Boehm titration method (Boehm 1994). This method gives both qualitative and quantitative information only about basic and acidic groups (in the form of carboxyl, lactone, and phenol). Basic groups can be distinguished by neutralization with HCl solution and acidic groups by NaHCO₃, Na₂CO₃ and NaOH solutions. In all the assays, standardized solutions of the chemical reagents (HCl, NaHCO₃, Na₂CO₃, and NaOH) were used. The acidic groups were determined by mixing 5 g of AC with 50 mL of solutions (0.1 N NaOH, 0.1 N NaHCO₃, or 0.1 N Na₂CO₃) in Erlenmeyer flasks (125 mL). The flasks were closed with PVC plastic film and shaken (Ethik Technology Brazil) for 24 h, at 140 rpm and 30 °C. The mixtures were filtered through a 0.45- μ m microporous membrane filter, and 10 mL aliquots were then taken by volumetric pipette from the filtrates, and were titrated with 0.1 N HCl solution. Subsequently, the aliquots were acidified by the addition of 5 mL of 0.1 N HCl solution, and then were back-titrated with 0.1 N NaOH solution. Similarly, the basic sites were determined by mixing 2 g of AC with 20 mL of 0.1 N HCl solution. From the obtained solutions, 10 mL aliquots were taken by volumetric pipette, then were titrated with 0.1 N NaOH solution; the aliquots were alkalized by the addition of 5 mL of 0.1 N NaOH solution, and then were back-titrated with 0.1 N HCl solution. The numbers of acidic sites of various types were calculated under the assumption that NaOH neutralizes the carboxyl, phenolic, and lactonic groups; Na₂CO₃–carboxyl and lactonic groups; and NaHCO₃ only carboxyl groups. The number of surface basic sites was calculated from the amount of HCl which reacted with AC. Neutralization points were known using pH indicators of phenolphthalein solution (0.1%) for titration of strong base and strong acid, while methyl red solution (0.1%) was used for the titration of weak base and strong acid. All determinations were processed in duplicate. The values of point of zero charge (pH_{PZC}) were estimated by pH measurements before and after contact with the AC, according to the method described by Regalbuto and Robles (2004). A fixed weight of 0.05 g of the AC was put into a series of 125-mL Erlenmeyer flasks (11 points) with 100 mL HCl or NaOH solution (initial pH adjusted from 2.0 to 12.0).

The flasks were closed with a PVC plastic film. After being shaken for 24 h using an orbital shaking incubator (Ethik Technology Brazil) at 120 rpm and 28 °C, the final pH value of each flask was measured using a pH meter (Hanna, Instruments Inc.). The difference between initial and final pH (ΔpH) was plotted against initial pH and the point at which $\Delta\text{pH} = 0$ was recorded as the pH_{PZC} value.

Textural properties

The complete isotherms of nitrogen (77 K) were measured in the range of relative pressures of (P/P^0) of 10^{-6} to 1. The BET Nova 1200e Surface Area and Pore Size Analyzer equipment (Quantacrome) was used. The samples were previously treated under vacuum at 300 °C for 3 h. The specific surface area (S_{BET}) was calculated from the isotherms using the Brunauer-Emmett-Teller (BET) equation (Sing 1989). The total volume of pores (V_T) was calculated as the maximum amount of nitrogen adsorbed to the relative pressure (P/P^0) of 0.99. The Dubinin-Radushkevich (DR) method was used to calculate the micropore volume (V_{MIC}) (Dubinin 1960). The mesopore (V_{MES}) and macropore (V_{MAC}) volumes were calculated using the experimental data from the mercury intrusion porosimetry analysis. These data were measured with the AutoPore IV 9500 V1.09 (Micromeritics) at maximum pressure of 5000 psi.

Batch adsorption experiments

Batch adsorption experiments were carried out in Erlenmeyer flasks (250 mL) containing 0.7 g of AC (AC-R1 or AC-R2) and 100 mL of BB26 solution with initial concentration in the range of 0.099 to 0.790 mmol L⁻¹. The flasks were placed in a thermostatically controlled orbital shaker (Ethik Technology Brazil), at constant stirring speed of 120 rpm, contact time of 24 h, and at required temperature. The samples were withdrawn at suitable time intervals (20 min) and filtered through a 0.45- μm microporous membrane filter. All assays were processed in duplicate and distilled water (pH 6.8–7.2) was used. The initial and equilibrium concentrations of the BB26 dye were measured at a wavelength of 618 by using UV/visible spectrophotometry (Bioespectro SP-220 Brazil). Adsorption experiments were conducted by using dye solutions at an initial pH of 5.8, adjusted with HCl solution (0.1 M) and the pH values were measured with a pH meter (Hanna, Instruments Inc.). The initial pH value of the dye solution was fixed based on the pH_{PZC} values of the adsorbents ($\text{pH}_{\text{PZC}} = 3.6$ for AC-R1 and $\text{pH}_{\text{PZC}} = 3.9$ for AC-R2), and pKa value of the BB26 dye (pKa 8.3) (Kumar and Tamilarasan 2013; Anirudhan et al. 2014).

Effect of the initial dye concentration on sorption capacity

The experiments were carried out using the BB26 solution with initial concentration in the range from 0.099 to 0.790 mmol L⁻¹, at 28 °C, and keeping all other variables constant. The flasks were agitated until the equilibrium was reached and the BB26 concentrations were determined. The quantity of adsorbed dye per adsorbent mass unit (q_e , mg g⁻¹) and the removal percentage of dye from the solutions were calculated using the Eqs. 1 and 2, respectively:

$$q_e = \frac{(C_0 - C_e)}{m} \cdot V \quad (1)$$

$$\text{Removal (\%)} = \frac{(C_0 - C_e)}{C_0} \cdot 100 \quad (2)$$

where C_0 is the initial concentration of dye in the solution (mmol L⁻¹), C_e is the equilibrium dye concentration in the solution (mmol L⁻¹), V is the solution volume (L), and m is the adsorbent mass (g).

Adsorption kinetics

In the adsorption kinetic study, the BB26 solution with initial concentration of 0.494 mmol L⁻¹, temperature of 28 °C, and contact times of 5, 15, and 30 min, and 1, 2, 3, 4, 5, 6, 8, 12, and 24 h were used, keeping all other variables constant. In order to analyze the kinetics involved in the adsorption processes of BB26 by ACs, the kinetic models of pseudo-first order (Lagergren 1898) and pseudo-second order (Ho and McKay 1998) were tested.

The pseudo-first-order equation is the most widely used rate equation in liquid-phase sorption processes; it is based on solid capacity, and it is generally expressed as Eq. 3. Integrating this equation for the boundary conditions $t = 0$ to $t = t$, and $q = 0$ to $q = q_t$, and thus Eq. 4 is obtained:

$$\frac{dq}{dt} = k_1(q_e - q) \quad (3)$$

$$q_t = q_e [1 - \exp(-k_1 t)] \quad (4)$$

The pseudo-second-order equation is based on the adsorption capacity, which may be expressed in the form of Eq. 5. Integrating this equation for the boundary conditions $t = 0$ to $t = t$ and $q = 0$ to $q = q_t$, then an expression in form of Eq. 6 is obtained:

$$\frac{dq}{dt} = k_2(q_e - q)^2 \quad (5)$$

$$q_t = \frac{k_2 \cdot q_e^2 \cdot t}{1 + (q_e k_2 t)} \quad (6)$$

The intraparticle diffusion model (Weber and Morris 1963) is used to identify the diffusion mechanism. According to this theory, the adsorbed amount (q_t) varies almost proportionally with the square root of the contact time, $t^{1/2}$ rather than t (Eq. 7):

$$q_t = k_i t^{1/2} + C \tag{7}$$

In order to predict if the rate-limiting step of adsorption is film diffusion or particle diffusion, the kinetic data were analyzed by using the Boyd equation (Boyd et al. 1947) (Eq. 8). Although the equation proposed by Boyd et al. (1947) assumes constant concentration outside the particle (infinite volume), it has been widely employed to describe surface diffusion in batch reactors (Andrade et al. 2018):

$$B_t = -\ln\left(1 - \frac{q_t}{q_e}\right) - 0.4977 \tag{8}$$

where q_t is the amount of dye adsorbed at time t (mmol g^{-1}), q_e is amount of dye adsorbed at equilibrium (mmol g^{-1}), t is the contact time (min), k_1 is the rate constant of the pseudo-first-order adsorption (min^{-1}), k_2 is the rate constant of the pseudo-second-order adsorption ($\text{g mmol}^{-1} \text{min}^{-1}$), k_i is the intraparticle diffusion constant ($\text{mmol g}^{-1} \text{min}^{-1/2}$), and C is a constant related to the thickness of the limit layer (mmol g^{-1}) evaluated.

The parameters of the kinetic models were estimated by nonlinear regression, and the fit quality was evaluated by adjusted determination coefficient (R^2_{adj}) that was calculated by Eq. 9, while the parameter R^2 was estimated by using Eq. 10 (Dotto et al. 2013):

$$R^2_{\text{Adj}} = 1 - (1 - R^2) \frac{n-1}{p-1} \tag{9}$$

$$R^2 = \left[\frac{\sum_i^n (q_{i,\text{exp}} - \bar{q}_{i,\text{exp}})^2 - \sum_i^n (q_{i,\text{exp}} - q_{i,\text{model}})^2}{\sum_i^n (q_{i,\text{exp}} - \bar{q}_{i,\text{exp}})^2} \right] \tag{10}$$

where R^2 is the determination coefficient, n is the number of experiments performed, p is the number of parameters of the fitted model, $q_{i,\text{model}}$ is each value of q predicted by the fitted model, $q_{i,\text{exp}}$ is each value measured experimentally, and $\bar{q}_{i,\text{exp}}$ is the average of the values of q measured experimentally.

Adsorption equilibrium

The adsorption equilibrium assays were performed at 28, 35, and 45 °C, initial BB26 concentration from 0.099 to 0.494 mmol L^{-1} , and keeping all other variables constant. The Langmuir (Langmuir 1918) and Freundlich (Freundlich 1906) models were adjusted to the experimental data, Eqs. 11 and 12, respectively. The parameters of the kinetic models

were estimated by nonlinear regression. The dimensionless constant separation factor, R_L was calculated using Eq. 13; their values indicate: irreversible adsorption ($R_L = 0$), favorable ($0 < R_L < 1$), and linear or non-favorable ($R_L > 1$) (Hall et al. 1966):

$$q_e = \frac{K_L q_m C_e}{1 + K_L C_e} \tag{11}$$

$$q_e = K_F \cdot C_e^{1/n} \tag{12}$$

$$R_L = \frac{1}{1 + K_L C_0} \tag{13}$$

where q_m is the maximum adsorption capacity (mmol g^{-1}), K_L is the Langmuir constant related to the affinity between adsorbent and adsorbate (L mmol^{-1}), K_F is Freundlich constant ($(\text{mmol g}^{-1}) (\text{L mmol}^{-1})^{1/n}$), and $1/n$ is the Freundlich intensity parameter which indicates the magnitude of the adsorption driving force or surface heterogeneity; the n values in the range $1 < n < 10$ characterize favorable adsorption.

Adsorption thermodynamic parameters

The thermodynamic parameters were investigated by experimental data obtained from adsorption experiments of BB26 onto ACs (AC-R1 and AC-R2) at different temperatures (28, 35, and 45 °C). The standard values of Gibbs free energy change (ΔG^0 , kJ mol^{-1}) were calculated using Eq. 14, while the values of standard enthalpy change (ΔH^0 , kJ mol^{-1}) and entropy change (ΔS^0 , $\text{kJ mol}^{-1} \text{K}^{-1}$) were estimated from the slope and intercept of a plot of $\ln K_D$ against $1/T$ (Eq. 15) (Bhattacharyya et al. 2014; Anastopoulos and Kyzas 2016):

$$\Delta G^0 = -RT \ln(K_D) \tag{14}$$

$$\ln(K_D) = \frac{\Delta S^0}{R} - \frac{\Delta H^0}{RT} \tag{15}$$

where K_D is the thermodynamic equilibrium constant. K_D was calculated as a dimensionless parameter by multiplying ($K_d = q_e/C_e$), distribution constant (L g^{-1}) by (ρ_w), water density (10^3 g L^{-1}) for values of q_e (mol g^{-1}) and C_e (mol L^{-1}). R is the universal gas constant ($8.314 \text{ J mol}^{-1} \text{K}^{-1}$), T is the temperature (K) (Liu 2009).

Results and discussion

Physicochemical properties of the AC samples

The values of ash and moisture content for the AC samples are, respectively: AC-R1 (0.02 and 2.06%) and AC-R2 (0.02 and 4.21%). The ash content depends on the chemical composition of the precursors (mainly inorganic compounds) and of the experimental conditions of the activating process

(Yakout et al. 2013). Typical values are 2–3% wt for coconut shell-based AC, 5% wt for wood-based AC, and 18–15% wt for coal-based AC. The chemical characteristics represented by ash content, pH, and conductivity can affect the use of an AC for specific applications. For instance, the adsorption of organic compounds, like methylene blue and phenol; high surface area; high bulk density; neutral pH; low ash; and low conductivity were found to be desirable characteristics (Ahmed and Theydan 2012). According to Liou (2010), the ash content removal of the raw materials by an adequate base-leaching step (to avoid obstructing the pore development), increases the S_{BET} of the AC. The moisture content does not adversely affect the AC performance in adsorption; it merely acts as diluents. However, water molecules adsorbed on the primary center can prevent adsorbate access to hydrophobic regions on the activated carbon surface and/or effectively block adsorbate access to the micropores (Yakout et al. 2013).

The XRD patterns of AC-R1 and AC-R2 are shown in Fig. 2. Two peaks of different intensities for both ACs, indicating similar structures, can be observed. The peaks are located around $2\theta = 25^\circ$ and $2\theta = 43^\circ$. The first one can be attributed to a disordered carbon structure, and the second to organized carbon. Therefore, the peaks indicate an amorphous structure (Saygili and Guzel 2016).

The FT-IR spectra of AC-R1 and AC-R2 are presented in Fig. 3. Both spectra were similar and the same vibrational bands were observed. The broad band at around 3500 cm^{-1} indicates the vibration of the O-H stretch. This can be attributed to hydroxyl groups from carboxyls, phenols or alcohol, and physically adsorbed water (Kumar and Jena 2016; Sahu et al. 2010; Gao et al. 2011). The bands at 1630 cm^{-1} are characteristic of C=O stretching vibrations of ketones, aldehydes, lactones, or carboxyl groups (Mourão et al. 2011). A sharp peak at 1550 cm^{-1} corresponds to an aromatic ring structure, which assigns to the presence of phenolic groups. The broad band at around 1180 cm^{-1} can be associated to the

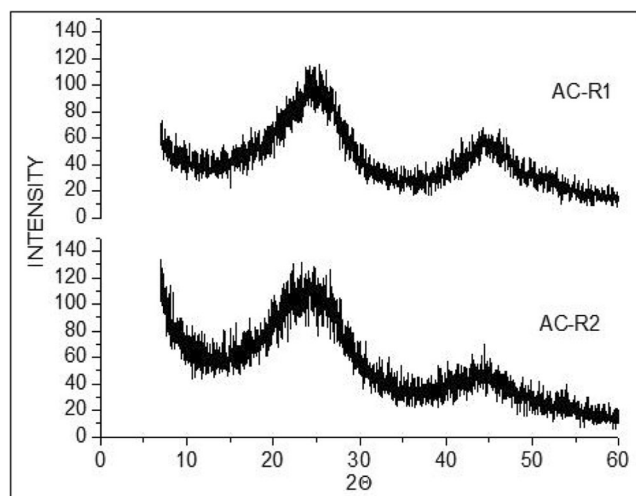


Fig. 2 XRD patterns for AC-R1 and AC-R2

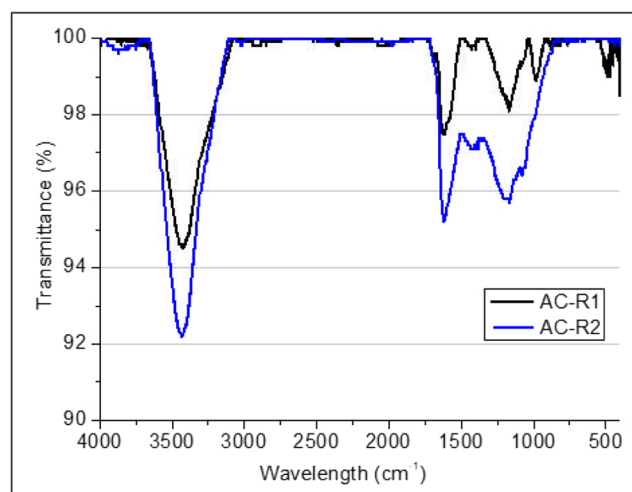


Fig. 3 FT-IR spectra of ACs (AC-R1; AC-R2)

C–O stretching of ethers, lactones, and phenols (Attia et al. 2006).

Acid-base characteristics

The quantities (mEq g^{-1}) of acidic and basic functional groups and the pH_{PCZ} values are shown in Table 1. From the Boehm method, quantitative data are obtained on the functional groups present on the surface of activated carbon, such as lactonic, phenolic, and carboxylic acid groups. On the surfaces of the ACs occur the predominance of total acidic surface groups, as 3.78 mEq g^{-1} (AC-R1) and 3.87 mEq g^{-1} (AC-R2). The amount of total acidic surface groups is around 18 to 35-fold excess higher compared to the total basic surface groups, for AC-R1 and AC-R2, respectively. The ACs contain the same acidic groups near each other on their surface. The type of precursor did not significantly affect the type and amount of the acidic surface groups of the ACs. Conversely, the amount of basic surface groups of the AC-R2 was about 50% lower than that of AC-R1. The ACs presented an increase of oxygenated groups, and consequently a decrease of the pH_{PCZ} (Table 1). The pH_{PZC} values for the AC samples (pH_{PZC} 3.6 for A-R1 and pH_{PZC} 3.9 for AC-R2) indicated that the adsorbent surfaces have acidic character. These results are

Table 1 Acid-base characteristics of the AC samples

Parameter	AC-R1	AC-R2
pH_{PZC}	3.6	3.9
Carboxylic ($-\text{COOH}$) (mEq g^{-1})	1.32	1.31
Phenolic ($-\text{OH}$) (mEq g^{-1})	1.69	1.86
Lactones ($-\text{COOR}$) (mEq g^{-1})	0.77	0.70
Total AG (mEq g^{-1})	3.78	3.87
Total BG (mEq g^{-1})	0.21	0.11

in agreement with the FT-IR spectra (Fig. 3), which showed the presence of acidic surface groups, as carboxyl and phenolic on the AC surfaces.

The solution pH plays an important role in the dye adsorption onto AC. This parameter affects the surface characteristics of the ACs (surface functional groups) and the degree of ionization of the dye. The pH_{PZC} is defined as the pH value at which the net surface charge (external and internal) is zero (Tran et al. 2017). The adsorption characteristics of an adsorbent can be obtained from pH_{PZC} determination (Katarzyna et al. 2007). Thus, at solution $pH > pH_{PZC}$, the surfaces of ACs are negatively charge, which provides electrostatic interactions that are favorable for adsorbing cationic species. In addition, at solution $pH < pK_a$, the BB26 molecule (pK_a 8.3) is in ionized form as a cationic species. According to Crini and Badot (2008), basic dye, as BB26 dye, has high positive charge density at a low pH. At low pH values (solution $pH < pH_{PZC}$), both positively charged BB26 molecules and H^+ ions presented in solution compete with each other for adsorption on the active sites of ACs (Hameed et al. 2008a).

Textural properties

The values of specific superficial area (S_{BET}) of AC-R1 and AC-R2 were of 990.81 and 1651.31 $m^2 g^{-1}$, respectively. The ACs have microporous structures, according to the following distribution of pores for AC-R1 (V_T 0.722 $cm^3 g^{-1}$, V_{MES} 21.45%, and V_{MIC} 71.69%) and AC-R2 (V_T 1.194 $cm^3 g^{-1}$, V_{MES} 8.57%, and V_{MIC} 91.31%). Under the same experimental conditions, the S_{BET} and V_{MIC} values for AC-R1 were lower than that the values of AC-R2. The S_{BET} and pore volume values of the AC samples were compared to the other results given in the literature (Table 2); the high-quality activated carbons that were prepared from açai stones (AC-R1) and Brazil nut shells (AC-R2) can be observed. The values are comparable to the ACs produced by using different activators ($ZnCl_2$, NaOH, and H_3PO_4) and production methods as well as precursors which are potential raw materials to produce low-cost ACs.

In this study, the textural characteristics as S_{BET} and pore size distribution of the AC samples were found to be dependent on the precursor used. The differences probably arise due to the different constituents inherent in each precursor, including cellulose, hemicellulose, and lignin (Yeganeh et al. 2006; Liou 2010). In the production process of AC by activating with H_3PO_4 , pores are created due to the chemical reactions between the raw material biopolymers (cellulose and lignin) and the activating agent (Okada et al. 2003). The H_3PO_4 -activator promotes chemical change and structural alterations at lower temperature than those realized by physical activation (Jagtøyen and Derbyshire 1993). Additionally, the species such as H_3PO_4 , $H_4P_2O_7$, $H_5P_3O_{10}$, and some others, each one with a different molecular size, that occur in the activation

might cause a different distribution of micropore sizes in the resulting AC (Díaz-Díez et al. 2004). Chemical activation with H_3PO_4 is a useful technique for obtaining AC with desired pore size distribution from low-cost precursors at low temperature (Liou 2010; Ding et al. 2014; Lacerda et al. 2015). During the activating process, the H_3PO_4 -activator induces important changes in the pyrolytic decomposition of the lignocellulosic materials because it promotes depolymerization, dehydration, and redistribution of constituent biopolymers, favoring the conversion of aliphatic compounds to aromatic compounds at temperatures relatively low (around 400 to 500 °C) compared to the physical activating. Thus, it is an energy and time-saving scheme for AC production (Díaz-Díez et al. 2004). In the present study, a carbonization temperature of 450 °C was used; this aspect will contribute to the global cost reduction of the AC-R1 and AC-R2 production.

Adsorption experiments

Effect of the initial dye concentration

The effects of initial dye concentration were investigated under equilibrium conditions (Fig. 4). At C_0 of 0.10 $mmol L^{-1}$, the removal of BB26, for both ACs, attained a maximum value around 98.8%; this value slowly decreases to 98% of removal, at C_0 of 0.38 $mmol L^{-1}$, and q_e of 0.13 $mmol g^{-1}$. In the range of C_0 (0.38–0.79 $mmol L^{-1}$), the removal values decrease until 86% for AC-R1 and 88% for AC-R2, while the q_e values for AC-R1 and AC-R2 increase from 0.053 to 0.13 $mmol g^{-1}$, respectively. The results showed that the adsorption processes of BB26 onto ACs are depending, to a certain extent, on the initial dye concentration (C_0). These effects are explicated, at lower values of C_0 , the ratio between the initial number of dye molecules and the surface area of adsorbent available is low, and, because of that, the number of dye molecules in solution is adsorbed, in the case, the adsorption becomes independent of the value of C_0 . For high values of C_0 , the adsorption capacity (q_e) increases due to the increase in mass gradient between the solution and the adsorbent, which acts as a driving force for the transfer of dye molecules from solution to the adsorbent surface. The ratio between the initial number of dye molecules and the surface area available is high; so, the adsorption sites quickly saturate, and their number is reduced, then the adsorption rate decreases and, consequently, a larger number of dye molecules remains in the solution for an established equilibrium condition (Khan et al. 2012; Vimonses et al. 2009).

Adsorption kinetics

In order to characterize the kinetics involved in the adsorption processes of BB26 onto ACs, pseudo-first-order and pseudo-second-order kinetic models were fitted to experimental data,

Table 2 Comparison of AC-R1 and AC-R2 with other activated carbons from different precursors and activating conditions

Adsorbent	Activating agent	Carbonization temperature	S_{BET} ($\text{m}^2 \text{g}^{-1}$)	V_{T} ($\text{cm}^3 \text{g}^{-1}$)	V_{MIC} (%)	V_{MES} (%)	References
Macauba palm-carbon	ZnCl_2	900 °C/1.5 h	907	0.489	Not cited	90.40	Moura et al. (2018)
Palm kernel shell-carbon	ZnCl_2	550 °C/1 h	1223	0.700	Not cited	Not cited	Hidayu and Muda (2016)
Macauba palm endocarp-carbon	H_3PO_4	500 °C/1 h	296	0.201	61.19	Not cited	Lacerda et al. (2015)
Coconut shell-carbon	NaOH	700 °C/1.5 h	783	0.378	94.20	5.82	Cazetta et al. (2011)
Rice husk	H_3PO_4	500 °C/1 h	1543	2.480	Not cited	Not cited	Ding et al. (2014)
Sugar cane bagasse-carbon	H_3PO_4	500 °C/1 h	1543	0.999	19.11	69.67	Liou (2010)
Brazilian pine-fruit shell-carbon	H_2SO_4	100 °C/2 h	702	0.230	Not cited	Not cited	Royer et al. (2009)
Açai stone-carbon (AC-R1)	H_3PO_4	450 °C/2 h	990.81	0.722	71.69	21.45	Present work
Brazil nut shell-carbon (AC-R2)	H_3PO_4	450 °C/2 h	1651.31	1.194	91.31	8.57	Present work

and are shown in Fig. 5a, b, while the model parameters are presented in Table 3. The fit quality was based on the adjusted determination coefficient (R^2_{adj}) and comparison of the $q_{\text{e,exp}}$ (mmol g^{-1}) and $q_{\text{e,cal}}$ (mmol g^{-1}) values. As can be seen in Table 3, the pseudo-second-order model was found to be well-fitted to experimental data, and was suitable to describe the adsorption dynamics. The pseudo-second-order model presented highest values of R^2_{adj} (0.9525–0.9747) as well as the $q_{\text{e,cal}}$ values (0.0793 mmol g^{-1} for AC-R1 and 0.0814 mmol g^{-1} for AC-R2) were near to the $q_{\text{e,exp}}$ values (0.0803 mmol g^{-1} for AC-R1 and 0.0827 mmol g^{-1} for AC-R2). The pseudo-first-order model was not suitable to describe the experimental data, for both adsorption processes, because the R^2_{adj} and $q_{\text{e,cal}}$ values were lowest than that of the pseudo-second-order model, for AC-R1 (R^2_{adj} 0.9233; $q_{\text{e,cal}}$ 0.0733 mmol g^{-1}) and AC-R2 (R^2_{adj} 0.9649; $q_{\text{e,cal}}$ 0.0612 mmol g^{-1}). Therefore, the adsorption processes of

BB26 onto ACs (AC-R1 and AC-R2) follow the pseudo-second-order kinetic model. The results are in good agreement with those about adsorption of basic blue 26 (BB26) onto fly ash, from the analysis carried out by Ho and McKay (1999) on the basis of the pseudo-second-order rate mechanism.

The possibility of intraparticle diffusion was examined by using the intraparticle diffusion model. It assumes that the adsorption mechanism occurs through the diffusion of the adsorbate into the pores of the adsorbent solid. The plot q_t vs. $t^{1/2}$ shows multi-linearity, and each linear portion represents a distinct mass transfer mechanism (Weber and Morris 1963). Furthermore, if the regression passes through the origin, then the rate-limiting process is only due to the intraparticle diffusion. Otherwise, the intraparticle diffusion is not the only rate-controlling step and some degrees of boundary layer diffusion also control the adsorption process. The straight line slope corresponds to intraparticle diffusion constant (k_i , $\text{mmol g}^{-1} \text{min}^{-1/2}$) and the intercept corresponds to value of C (mmol g^{-1}). The value of C (mmol g^{-1}) give an indication about the thickness of the boundary layer. For adsorption processes of BB26 onto ACs, the plots of q_t vs. $t^{1/2}$ are shown in Fig. 6a, b; the results suggest that the adsorption processes follow three stages. The stage (I) is attributed to diffusion of BB26 to the external surface of the ACs, or the boundary layer effect at the initial stage of the adsorption. The stage (II) describes the intraparticle diffusion. The stage (III) describes reaching of dynamic equilibrium. For both adsorption processes, there is a linear relationship over a period of time (Table 3), on the basis of the R^2_{adj} values for AC-R1 and AC-R2, respectively (0.9678 and 0.9559). However, it did not pass through the origin, values of C for AC-R1 and AC-R2, respectively (0.9895 and 1.1838 mmol g^{-1}); this fact suggests that the intraparticle diffusion is present, but it is not the only rate-controlling step in adsorption processes, and other mechanisms might be involved (Hameed et al. 2008a; Cazetta et al. 2011). The plots of B_t vs. t of the Boyd's equation for adsorption of BB26 onto ACs present some linearity

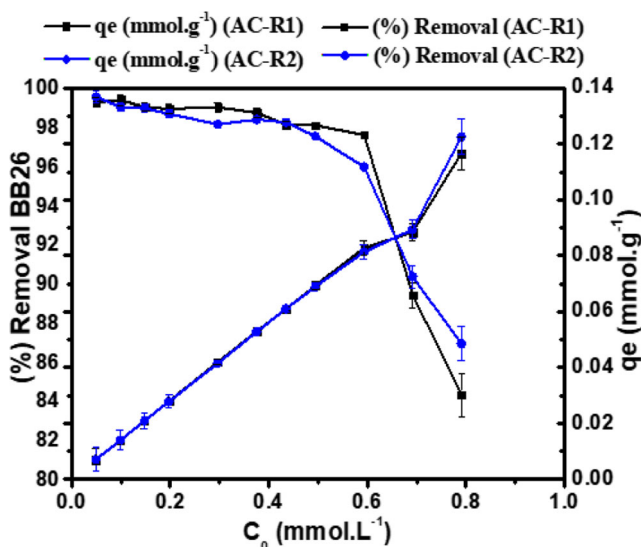


Fig. 4 Effect of the initial dye concentration on the adsorption capacity (q_{e} , mmol g^{-1}) and removal (%) of BB26 by ACs (AC-R1; AC-R2)

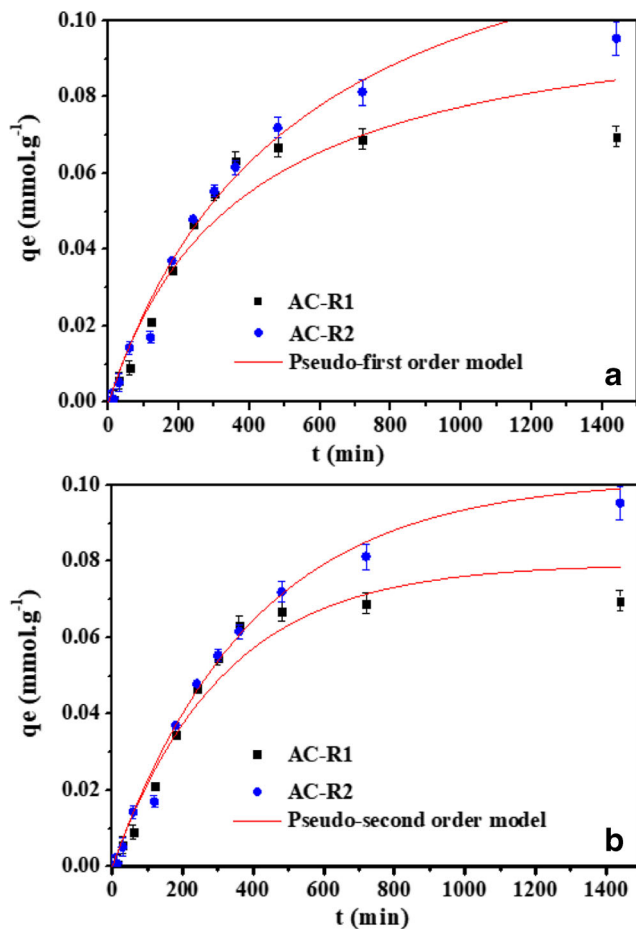


Fig. 5 Pseudo-first-order and pseudo-second-order kinetic models for adsorption of BB26 onto ACs, (T1 28 °C): a AC-R1 and b AC-R2

(Fig. 7a, b); however, not completely pass through the origin, and it suggests the involvement of film diffusion mechanisms (Hameed et al. 2008b). As can be seen in Fig. 7a, b, at higher contact time values, the experimental data are more scattered, which supports the assumption that film diffusion is a rate-

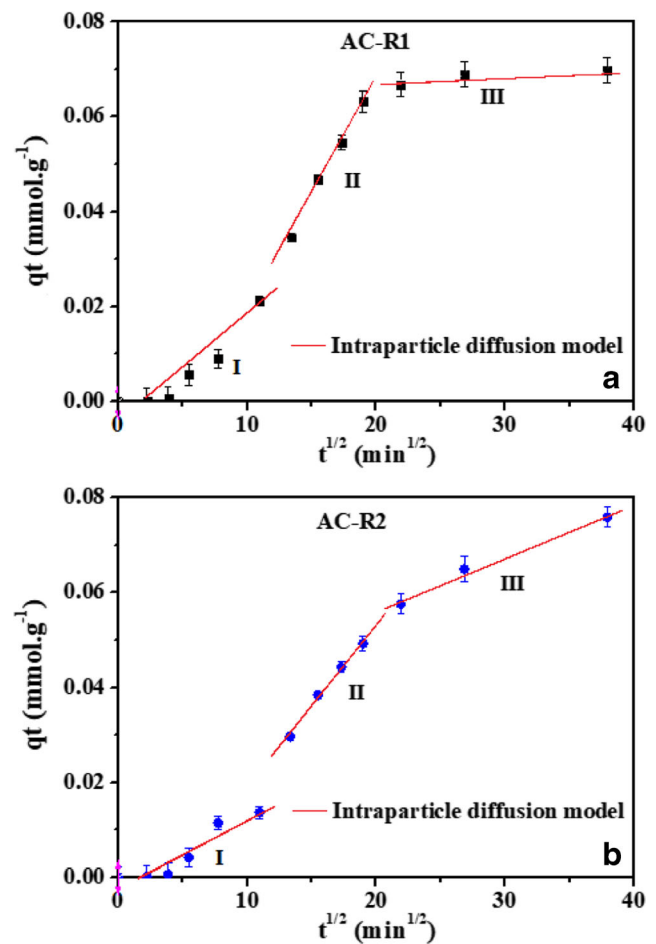


Fig. 6 Intraparticle diffusion model for adsorption of BB26 onto ACs, (T1 28 °C): a AC-R1 and b AC-R2

controlling step in adsorption processes (Martins et al. 2015; Andrade et al. 2018).

Adsorption equilibrium

With respect to the adsorption of BB26 by ACs, the Langmuir and Freundlich isotherm models were fitted to the experimental data. The equilibrium model parameters are presented in Table 4, and the R^2_{adj} values were used in order to determine the best fit. The Langmuir model was the most suitable to describe the experimental data of the adsorption of BB26 onto ACs (AC-R1 and AC-R2), on the basis of the R^2_{adj} values (Table 4). Figure 8a, b shows the fittings of the experimental data to the Langmuir isotherm model. The Langmuir model assumes that adsorption occurs in a monolayer, where the active sites are identical and energetically equivalent, that there are no interactions between the adsorbed molecules, and that no transmigration of the adsorbed molecules takes place on the adsorption surface, that corresponds to the so-called ideal localized monolayer (Langmuir 1918). This model, despite its obvious imperfections, occupies a central

Table 3 Parameters of the adsorption kinetic models

Model	Parameters	AC-R1	AC-R2
Pseudo-first order	$q_{e, \text{exp}}$ (mmol g ⁻¹)	0.0803	0.0827
	$q_{e, \text{cal}}$ (mmol g ⁻¹)	0.0733	0.0612
	k_1 (min ⁻¹)	0.0063	0.0050
	R^2_{adj}	0.9233	0.9649
Pseudo-second order	$q_{e, \text{cal}}$ (mmol g ⁻¹)	0.0793	0.0814
	k_2 (g mmol ⁻¹ min ⁻¹)	0.1061	0.1175
	R^2_{adj}	0.9525	0.9747
Intraparticle diffusion	C (mmol g ⁻¹)	0.9895	1.1838
	k_f (mmol g ⁻¹ min ^{-1/2})	1.2321	1.1339
	R^2_{adj}	0.9678	0.9559

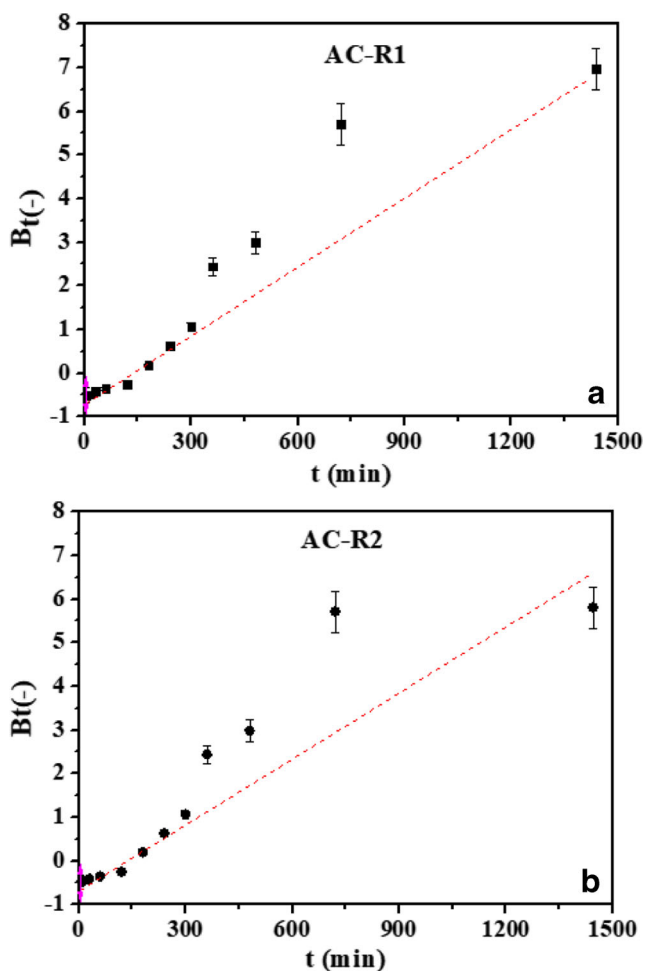


Fig. 7 Boyd plot for adsorption of BB26 onto ACs (T1 28 °C): **a** AC-R1 and **b** AC-R2

position in surface and adsorption science (Ruthven 1984; Dabrowski 2001).

The results suggest that both adsorption processes were monolayer adsorption; the adsorption capacity values (q_m) were found to be 0.0959 mmol g⁻¹ (28 °C), 0.1038 mmol g⁻¹ (35 °C), and 0.1007 mmol g⁻¹ (45 °C) for AC-R1, and 0.1011 mmol g⁻¹ (28 °C), 0.1029 mmol g⁻¹ (35 °C), and 0.1066 mmol g⁻¹ (45 °C) for AC-R2. The R_L

values (Table 4) confirm that the BB26 adsorption is favorable, with values below 1, for both cases. The Langmuir constant values (K_L) decreased with the increase of the temperature, and this result indicates thermodynamic consistency of the experimental data, and that the adsorption processes are exothermic. The q_m values for BB26 onto AC-R2 slightly rise with increase of temperature from 28 to 45 °C, while the q_m values for AC-R1 are practically constant in the temperature range of the investigation. The adsorption capacity values (q_m) of ACs for BB26 dye were compared to some other adsorbents reported in literature (Table 5). From Table 5, the values of q_m for the ACs (AC-R1 and AC-R2) are higher than that of the majority of the other adsorbents cited; only the photocatalyst (iron-doped titania/silane) shows superior performance in comparison to the adsorbents presented. It should be emphasized that the data of BB26 adsorption are limited from literature. Nonetheless, it should be noted that an accurate comparison is not feasible in this case, given the differences observed from the experimental conditions of the adsorption assays and characteristics of the adsorbents.

The adsorption isotherms (Fig. 8a, b) can be classified as L2 type (Giles et al. 1974). In the adsorption process where such isotherm is obtained, the adsorption of solute onto the adsorbent proceeds until a monolayer is established; the formation of further layers is not possible in this case. L2-type isotherm is usually associated with ionized solute adsorption with weak competition with the solvent molecules, and it is indicative of high affinity between the adsorbate and adsorbent surface (Giles et al. 1960). The removal of BB26 by ACs from aqueous solution effectively occurs at low equilibrium concentrations, according to the inclined portion from the isotherms (Fig. 8a, b), which indicates high affinity between the AC surfaces and BB26 dye. On the other hand, at higher equilibrium concentrations, both isotherms reach a maximum capacity as indicated by the plateau of the data. Because of the L2 type curve shape, the Langmuir model is appropriate to describe the experimental data of adsorption equilibrium.

A possible interaction mechanism for adsorption of BB26 onto ACs (AC-R1 and AC-R1) is proposed on the basis of the effects of the solution chemistry (pH effect),

Table 4 Parameters of the adsorption equilibrium models

	Langmuir					Freundlich		
	T (°C)	q_e (mmol L ⁻¹)	K_L (L mmol ⁻¹)	R^2_{adj}	R_L	n	K_f ((mmol g ⁻¹)(L mmol ⁻¹) ^{1/n})	R^2_{adj}
AC-R1	28	0.0959	225.59	0.9950	0.0055	4.27	0.1885	0.8889
	35	0.1038	189.08	0.9910	0.0066	3.34	0.2237	0.8849
	45	0.1007	162.08	0.9818	0.0077	3.05	0.2387	0.9564
AC-R2	28	0.1011	232.86	0.9820	0.0054	3.56	0.2090	0.8474
	35	0.1029	166.62	0.9486	0.0075	3.59	0.1937	0.7947
	45	0.1066	100.24	0.9575	0.0124	3.13	0.2123	0.8454

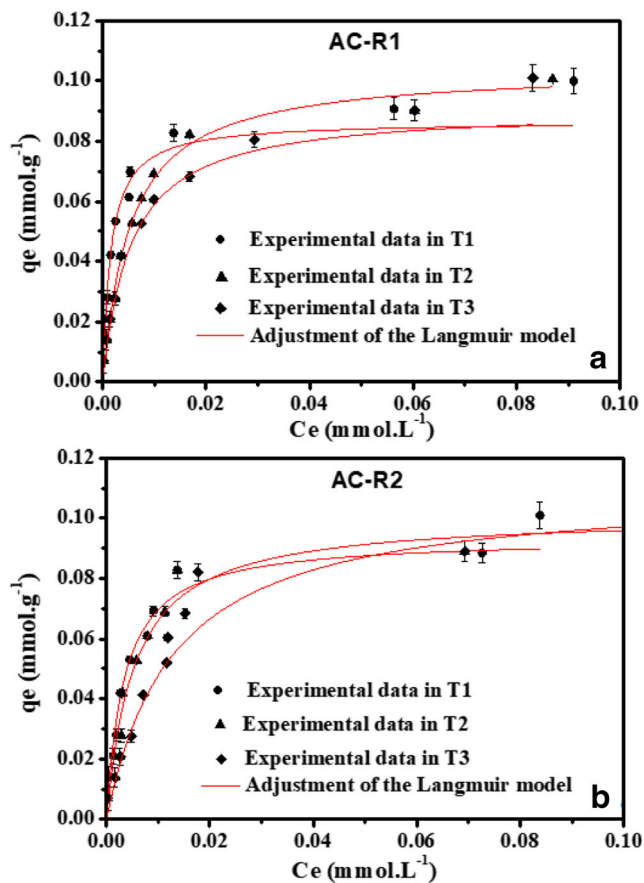


Fig. 8 Adsorption isotherms of BB26 onto ACs (T1 28 °C, T2 35 °C, T3 45 °C): **a** AC-R1 and **b** AC-R2

characteristics of ACs and BB26 molecules, previous study with respect to adsorption of BB26 onto AC-R1 and AC-R2 (Souza et al. 2018), and other results from literature. A study with respect to global molecular reactivity of basic dyes, and the adsorption of basic dyes onto ACs was performed by Souza et al. (2018). The results concerning the adsorption of BB26 onto ACs indicated that the BB26 molecules were significantly adsorbed onto ACs produced by physical and chemical (AC-R1 and AC-R1) activating; however, it was not adsorbed onto ACs oxidized with nitric acid (HNO₃). According to Radovic

et al. (1997), the carbon–oxygen functional groups present on the AC surfaces are by far the most important structures that influence the surface characteristics and behaviors of the ACs in adsorption. They not only lower pHPZC of the ACs, but they also reduce the dispersive adsorption potential by decreasing the π-electron density in the graphene layers; consequently, adsorption potential by electrostatic interactions increases. During the adsorption of BB26 dye onto acid AC surfaces (AC-R1 and AC-R2), the electrostatic interactions appear when the BB26 molecules are dissociated in aqueous solution (cationic form) and the surfaces of the ACs are negatively charged, as a pH effect of the solution. The negative charge on the AC surfaces results from the dissociation of surface oxygen complexes of acid character, such as carboxyl and phenolic groups (Moreno-Castilla 2004). Therefore, at initial pH 5.8, near to the pHPZC values of ACs (3.6 for AC-R1 and 3.9 for AC-R2), BB26 (in the cationic form) is the predominant species in solution (Crini and Badot 2008), as solution pH 5.8 > pHPZC, the AC surfaces are negatively charged. In this case, during the adsorption, solution pH increases toward the pKa value of BB26 (8.3), and then the BB26 molecules (cationic form) are adsorbed until near to the pKa (8.3). At solution pH > pKa, the concentration of cationic BB26 decreases, because BB26 in the molecular form (not ionized) is the predominate species in solution. Consequently, near to the pKa value (8.3), a point of equilibrium is reached and the maximum adsorption capacity is observed. On the basis of the mechanism presented, optimum adsorption of BB26 onto ACs by electrostatic interaction mechanism should occur at pH values between 4.0 and 8.0. Previous studies have shown that maximum adsorption of BB26 dye onto fly ash occurred at pH 8.0 (Khare et al. 1987), the optimum removal of BB26 by carbon/Zn/alginate polymer bead at pH 5.0 (Kumar and Tamilarasan 2013), and maximum adsorption of BB26 onto poly(IA-co-AMPS)Fe-TiO₂/MPTMS at pH 6.5 (Anirudhan et al. 2014). In the adsorption processes of BB26 by AC-R1 and AC-R2, the effects of mass transfer (processes controlled by film diffusion) and solution pH (surface functionality of AC and dye molecule ionization)

Table 5 Comparison of BB26 maximum adsorption capacity onto ACs (AC-R1 and AC-R2) with other adsorbents

Adsorbent	q_m (mmol g ⁻¹) Langmuir	C_0 (mmol L ⁻¹)	pH (initial)	pHPZC	References
Fly ash	0.524×10^{-4}	0.100–0.850	8.0	2.4	Khare et al. (1987)
Carbon/Zn/alginate polymer composite beads	0.860×10^{-5}	0.008–0.039	Not cited	4.2	Kumar and Tamilarasan (2013)
Iron-doped titania/silane	0.304	0.049–0.198	Not cited	3.2	Anirudhan et al. (2014)
Carbon/Ba/alginate beads	0.770×10^{-5}	0.008–0.024	Not cited	5.2	Kumar et al. (2013)
AC-R1	0.096	0.099–0.494	5.8	3.6	Present work
AC-R2	0.101	0.099–0.494	5.8	3.9	Present work

Table 6 Thermodynamic parameters of the adsorption of BB26 onto AC-R1 and AC-R2

	ΔH^0 (kJ mol ⁻¹)	ΔS^0 (J mol ⁻¹ K ⁻¹)	ΔG^0 (kJ mol ⁻¹)		
			28 °C	35 °C	45 °C
AC-R1	-37.41	-33.05	-27.55	-27.01	-26.97
AC-R2	-42.82	-56.18	-26.00	-25.27	-24.11

corroborated the values of maximum adsorption capacity that were estimated from the adsorption equilibrium study.

Adsorption thermodynamic parameters

The negative values of Gibbs energy change (ΔG^0 , kJ mol⁻¹), at different temperatures (28, 35, and 45 °C) indicate that both adsorption processes, BB26 onto AC-R1 and AC-R2, are favorable and spontaneous (Table 6). The ΔG^0 values decreased with increasing temperature (-27.55, -27.01, and -26.97 kJ mol⁻¹ for AC-R1, and -26.00, -25.27, and -24.11 kJ mol⁻¹ for AC-R2), suggesting that the adsorption of BB26 onto ACs will be fewer favorable at higher temperature (Zhou et al. 2011). Adsorption of BB26 onto AC-R1 is more favorable when compared to those onto AC-R2. The ΔG^0 magnitude for physisorption is between -20 and 0 kJ mol⁻¹; chemisorption has a range -80–400 kJ mol⁻¹ (Kara et al. 2003); the values of ΔG^0 magnitude estimated from of adsorption processes were lower than that of those for chemisorption. The negative values of ΔH^0 for AC-R1 (-37.41 kJ mol⁻¹) and AC-R2 (-42.82 kJ mol⁻¹) indicate the exothermic nature of the BB26 adsorption. Additionally, the negatives values of ΔH^0 are in agreement with the results of the adsorption equilibrium study, in which the values of adsorption capacity (q_e) were found to be constants, and the equilibrium constant, K_L (Langmuir model), decreases with higher temperature conditions. On the other hand, if adsorption capacity increases as temperature increases, this reflects the endothermic nature of the adsorption process. The physical and chemical adsorption phenomena can be classified, to some extent, from the magnitude of the ΔH^0 value. The ΔH^0 values estimated for the BB26 adsorption are lower than bonding strengths of chemisorption ranging between 84 and 420 kJ mol⁻¹ (Crini and Badot 2008). According to Mattson and Mark (1971), the enthalpy of adsorption of organic molecules from aqueous solution on activated carbon is usually within the range 8 to 65 kJ mol⁻¹. The ΔH^0 values are in agreement with those of Ahmad and Kumar (2010) for malachite green onto treated ginger waste (47.49 kJ mol⁻¹), Gercel et al. (2008) for disperse dye onto biomass (plant material) (44.31 kJ mol⁻¹), Khattri and Singh (2009) for malachite green onto sawdust (-54.56 kJ mol⁻¹), Sulak et al. (2007) for Astrazon Yellow 7 onto wheat bran (46.81 kJ mol⁻¹), and Wang et al. (2009) chromium (VI) onto walnut hull

(65.14 kJ mol⁻¹). The negative ΔS^0 values (-33.05 J mol⁻¹ K⁻¹ for AC-R1 and -56.18 J mol⁻¹ K⁻¹ for AC-R2) confirm the decreased randomness at the solid-liquid interface during the adsorption. The less negative value of ΔS^0 found for BB26 onto AC-R2 reveals that a more ordered arrangement of BB26 molecules is shaped on the AC surface.

Conclusion

The H₃PO₄-activated carbons produced in this work presented high values of S_{BET} and porosity, comparable to others studies which used low-cost raw materials as precursors of AC. The S_{BET} values of the AC samples increased from 990.81 m² g⁻¹ (açai stones) to 1651.31 m² g⁻¹ (Brazil nut shells); the total pore volume and the micropore volume followed the same trend. The adsorption processes of BB26 onto ACs were found to follow the pseudo-second-order kinetic model. The intraparticle diffusion model and Boyd's equation were studied to evaluate the adsorption mechanisms; for both adsorption processes, the overall adsorption rates were found to be controlled by film diffusion. Equilibrium curves were L-type, and indicated high affinity between the adsorbents and basic dye at low equilibrium concentrations. Electrostatic interaction was found to be the mechanism dominant in the adsorptions processes attributed to the acidic character of AC surfaces. The Langmuir model was well-adjusted to the experimental data for both ACs, and the adsorption capacity values were found to be 0.0959 mmol g⁻¹ (28 °C), 0.1038 mmol g⁻¹ (35 °C), and 0.1007 mmol g⁻¹ (45 °C) for AC-R1, and 0.1011 mmol g⁻¹ (28 °C), 0.1029 mmol g⁻¹ (35 °C), and 0.1066 mmol g⁻¹ (45 °C) for AC-R2. The values of the separation factor R_L indicated favorable adsorption. The determination of the thermodynamic parameters indicates the spontaneous and exothermic nature of the adsorption processes. Thus, chemical activating with H₃PO₄ was able to generate materials with adequate characteristics for the adsorption purpose from açai stones and Brazil nut shells wastes. Additionally, the AC samples were effective toward removing BB26 from aqueous solutions.

Acknowledgments Authors acknowledge the financial support provided by Ministério da Ciência, Tecnologia e Inovação (MCTI)/Conselho Nacional de Desenvolvimento Científico e Tecnológico (CNPq)/Ministério da Educação (MEC)/Coordenação de Aperfeiçoamento de

Pessoal de Nível Superior (CAPES) - (CNPq/400624/2014-1-Casadinho/PROCAD) (Brazil).

Publisher's note Springer Nature remains neutral with regard to jurisdictional claims in published maps and institutional affiliations.

References

- Ahmad R, Kumar R (2010) Adsorption studies of hazardous malachite green onto treated ginger waste. *J Environ Manag* 91:1032–1038
- Ahmed MJ, Theydan SK (2012) Physical and chemical characteristics of activated carbon prepared by pyrolysis of chemically treated date stones and its ability to adsorb organics. *Powder Technol* 229:237–245
- Anastopoulos I, Kyzas GZ (2016) Are the thermodynamic parameters correctly estimated in liquid-phase adsorption phenomena? *J Mol Liq* 218:174–185
- Andrade JR, Silva MGC, Gimenes ML, Vieira MGA (2018) Bioadsorption of trivalent and hexavalent chromium from aqueous solutions by sericin-alginate particles produced from *Bombyx mori* cocoons. *Environ Sci Pollut Res* 25:25967–25982
- Anirudhan TS, Divya PL, Nima J, Sandeep S (2014) Synthesis and evaluation of Iron-doped titania/silane based hydrogel for the adsorptional photocatalytic degradation of Victoria blue under visible light. *J Colloid Interface Sci* 434:48–58
- Attia AA, Rashwan WE, Khedr SA (2006) Capacity of activated carbon in the removal of acid dyes subsequent to its thermal treatment. *Dyes Pigments* 69:128–136
- Aygun A, Yenisoay-Karakas S, Duman I (2003) Production of granular activated carbon from fruit stones and nutshells and evaluation of their physical, chemical and adsorption properties. *Microporous Mesoporous Mater* 66:189–195
- Bhattacharyya KG, Gupta SS, Sarma GK (2014) Interactions of the dye, Rhodamine B with kaolinite and montmorillonite in water. *Appl Clay Sci* 99:7–17
- Boehm HP (1994) Some aspects of the surface chemistry of carbon blacks and others carbons. *Carbon* 32:759–769
- Bonelli PR, Della Rocca PA, Cerrella EG, Cukierman AL (2001) Effect of pyrolysis temperature on composition, surface properties and thermal degradation rates of Brazil nut shells. *Bioresour Technol* 76:15–22
- Boyd GE, Adamson AW, Meyers LS (1947) The exchange adsorption of ions from aqueous solution by organic zeolites. II. Kinetics. *J Am Chem Soc* 69:2836–2848
- Cazetta AL, Vargas AMM, Nogamia EM, Kunita MH, Guilherme MR, Martins AC, Silva TL, Moraes JCG, Almeida VC (2011) NaOH-activated carbon of high surface area produced from coconut shell: kinetics and equilibrium studies from the methylene blue adsorption. *Chem Eng J* 174:117–125
- Crini G (2006) Non-conventional low-cost adsorbents for dye removal: a review. *Bioresour Technol* 97:1061–1108
- Crini G, Badot PM (2008) Application of chitosan, a natural aminopolysaccharide, for dye removal from aqueous solutions by adsorption processes using batch studies: a review of recent literature. *Prog Polym Sci* 33:399–447
- Dabrowski A (2001) Adsorption—from theory to practice. *Adv Colloid Interf Sci* 93:135–224
- Demiral H, Gungor C (2016) Adsorption of copper(II) from aqueous solutions on activated carbon prepared from grape bagasse. *J Clean Prod* 24:103–113
- Demirbas A (2009) Agricultural based activated carbons for the removal of dyes from aqueous solutions: a review. *J Hazard Mater* 167:1–9
- Deng H, Yang L, Tao G, Dai J (2009) Preparation and characterization of activated carbon from cotton stalk by microwave assisted chemical activation-application in methylene blue adsorption from aqueous solution. *J Hazard Mater* 166:1514–1521
- Díaz-Díez MA, Gómez-Serrano V, Fernández González C, Cuerda-Correa EM, Macías-García A (2004) Porous texture of activated carbons prepared by phosphoric acid activation of woods. *Appl Surf Sci* 238:309–313
- Ding L, Zou B, Gao W, Liu Q, Wang Z, Guo Y, Wang X, Liu Y (2014) Adsorption of Rhodamine-B from aqueous solution using treated rice husk-based activated carbon. *Colloids Surf A Physicochem Eng Asp* 446:1–7
- Dotto GL, Costa JAV, Pinto LAA (2013) Kinetic studies on the biosorption of phenol by nanoparticles from *Spirulina* sp. *LEB* 18. *J Environ Chem Eng* 1:1137–1143
- Dubinin MM (1960) The potential theory of adsorption of gases and vapors for adsorbents with energetically non-uniform surface. *Chem Rev* 60:235–266
- Forgacs E, Cserhádi T, Oros G (2004) Removal of synthetic dyes from wastewaters: a review. *Environ Int* 30:953–971
- Freundlich HMF (1906) Over the adsorption in solution. *J Phys Chem A* 57:385–470
- Gao P, Liu ZH, Xue G, Han B, Zhou MH (2011) Preparation and characterization of activated carbon produced from rice straw by $(\text{NH}_4)_2\text{HPO}_4$ activation. *Bioresour Technol* 102:3645–3648
- Geetha A, Palanisamy N (2016) Equilibrium and kinetic studies for the adsorption of Basic Red 29 from aqueous solutions using activated carbon and conducting polymer composite. *Desalin Water Treat* 57:8406–8419
- Gercel O, Gercel HF, Koparal AS, Ogutveren UB (2008) Removal of disperse dye from aqueous solution by novel adsorbent prepared from biomass plant material. *J Hazard Mater* 160:668–674
- Giles CH, Mc Ewen TH, Nakhwa SN, Smith D (1960) Studies in adsorption. Part XI. A system of classification of solution adsorption isotherms, and its use in diagnosis of adsorption mechanisms and in measurement of specific surface areas of solids. *J Chem Soc* 4:3973–3993
- Giles CH, Smith D, Huitson A (1974) A general treatment and classification of the solute adsorption isotherm I. Theoretical. *J Colloid Interface Sci* 47:755–765
- Gupta VK, Saleh TA (2013) Sorption of pollutants by porous carbon, carbon nanotubes and fullerene—an overview. *Environ Sci Pollut Res* 20:2828–2843
- Gupta VK, Suhas (2009) Application of low-cost adsorbents for dye removal—a review. *J Environ Manag* 90:2313–2342
- Gupta VK, Mohan D, Sharma S, Sharma M (2000) Removal of basic dyes (rhodamine B and methylene blue) from aqueous solutions using bagasse fly ash. *Sep Sci Technol* 35:2097–2113
- Haimour NM, Emeish S (2006) Utilization of date stones for production of activated carbon using phosphoric acid. *Waste Manag* 26:651–660
- Hall KR, Eagleton LC, Acrivos A, Vermeulen T (1966) Pore- and solid-diffusion kinetics in fixed-bed adsorption under constant-pattern conditions. *Ind Eng Chem Fundam* 5:212–223
- Hameed BH, Tan IAW, Ahmad AL (2008a) Adsorption isotherm, kinetic modeling and mechanism of 2,4,6-trichlorophenol on coconut husk-based activated carbon. *Chem Eng J* 144:235–244
- Hameed BH, Mahmoud DK, Ahmad AL (2008b) Equilibrium modelling and kinetic studies on the adsorption of basic dye by a low cost adsorbent: coconut (*Cocos nucifera*) bunch waste. *J Hazard Mater* 158:65–72
- Hidayu AR, Muda N (2016) Preparation and characterization of impregnated activated carbon from palm kernel shell and coconut shell for CO_2 capture. *Procedia Eng* 148:106–113
- Ho YS, McKay G (1998) Kinetic models for the sorption of dye from aqueous solution by wood. *Process Saf Environ Prot* 76:183–191

- Ho YS, McKay G (1999) Pseudo-second order model for sorption processes. *Process Biochem* 34:451–465
- Jagtøyen M, Derbyshire F (1993) Some considerations of the origins of porosity in carbons from chemically activated wood. *Carbon* 31: 1185–1192
- Kara M, Yuzer H, Sabah E, Celik MS (2003) Adsorption of cobalt from aqueous solutions onto sepiolite. *Water Res* 37:224–232
- Katarzyna SS, Krysztalkiewicz A, Jesionowski T (2007) Modification of hydrophilic/hydrophobic character of TiO₂ surface using selected silane coupling agents. *Physicochem Problem Miner Process* 41: 205–214
- Khan TA, Dahiya S, Ali I (2012) Use of kaolinite as adsorbent: equilibrium, dynamics and thermodynamic studies on the adsorption of Rhodamine B from aqueous solution. *Appl Clay Sci* 69:58–66
- Khare SK, Panday KK, Srivastava RM, Singh VN (1987) Removal of Victoria Blue from aqueous solution by fly ash. *J Chem Tech Biotechnol* 38:99–104
- Khattari SD, Singh MK (2009) Removal of malachite green from dye wastewater using neem sawdust by adsorption. *J Hazard Mater* 167:1089–1094
- Kumar A, Jena HM (2016) Preparation and characterization of high surface area activated carbon from Fox nut (*Euryale ferox*) shell by chemical activation with H₃PO₄. *Results Phys* 6:651–658
- Kumar M, Tamilarasan R (2013) Kinetics and equilibrium studies on the removal of Victoria Blue using *Prosopis juliflora*-modified carbon/Zn/alginate polymer composite beads. *J Chem Eng Data* 58:517–527
- Kumar M, Tamilarasan R (2014) Removal of Victoria Blue using *Prosopis juliflora* bark carbon: kinetics and thermodynamic modeling studies. *J Mater Environ Sci* 5:510–519
- Kumar M, Tamilarasan R, Sivakumar V (2013) Adsorption of Victoria Blue by carbon/Ba/alginate beads: kinetics, thermodynamics and isotherm studies. *Carbohydr Polym* 98:505–513
- Lacerda VS, Lopez-Sotelo JB, Correa-Guimarães A, Hernandez-Navarro S, Sanchez-Bascones M, Navas-Gracia LM, Martín-Ramos P, Martín-Gil J (2015) Rhodamine B removal with activated carbons obtained from lignocellulosic waste. *J Environ Manag* 155:67–76
- Lagergren S (1898) About the theory of so-called adsorption of soluble substance. *K Sven Vetenskapsakad Handl* 24:1–39
- Langmuir I (1918) The adsorption of gases on plane surfaces of glass, mica and platinum. *J Am Chem Soc* 40:1361–1403
- Liou T-H (2010) Development of mesoporous structure and high adsorption capacity of biomass-based activated carbon by phosphoric acid and zinc chloride activation. *Chem Eng J* 158:129–142
- Liu Y (2009) Is the free energy change of adsorption correctly calculated? *J Chem Eng Data* 54:1981–1985
- Martins AC, Pezoti O, Cazetta AL, Bedin KC, Yamazaki DAS, Bandoch GFG, Asefa T, Visentainer JV, Almeida VC (2015) Removal of tetracycline by NaOH-activated carbon produced from macadamia nut shells: kinetic and equilibrium studies. *Chem Eng J* 260:291–299
- Mattson JS, Mark HB (1971) *Activated carbon: surface chemistry and adsorption from solution*. Marcel Dekker, New York
- Mo J, Yang Q, Zhang N, Zhang W, Zheng Y, Zhang Z (2018) A review on agro-industrial waste (AIW) derived adsorbents for water and wastewater treatment. *J Environ Manag* 227:395–405
- Moreno-Castilla C (2004) Adsorption of organic molecules from aqueous solutions on carbon materials. *Carbon* 42:83–94
- Moura FCC, Rios RDF, Galvão BRL (2018) Emerging contaminants removal by granular activated carbon obtained from residual Macauba biomass. *Environ Sci Pollut Res* 25:26482–26492
- Mourão PAM, Laginhas C, Custódi F, Nabais JMV, Carrott PJM, Carrott MMLR (2011) Influence of oxidation process on the adsorption capacity of activated carbons from lignocellulosic precursors. *Fuel Process Technol* 92:241–246
- Nethaji S, Sivasamy A, Thennarasu G, Saravanan S (2010) Adsorption of Malachite Green dye onto activated carbon derived from *Borassus aethiopum* flower biomass. *J Hazard Mater* 181:271–280
- Okada K, Yamamoto N, Kameshima Y, Yasumori A (2003) Adsorption properties of activated carbon from waste newspaper prepared by chemical and physical activation. *J Colloid Interface Sci* 262:194–199
- Prauchner MJ, Rodríguez-Reinoso F (2012) Chemical versus physical activation of coconut shell: a comparative study. *Microporous Mesoporous Mater* 152:163–171
- Przystaś W, Zabłocka-Godłowska E, Grabińska-Sota E (2012) Biological removal of azo and triphenylmethane dyes and toxicity of process by-products. *Water Air Soil Pollut* 223:1581–1592
- Radovic LR, Silva IF, Ume JI, Menéndez JA, Leon y Leon CA, Scaroni AW (1997) An experimental and theoretical study of the adsorption of aromatics possessing electron-withdrawing and electron-donating functional groups by chemically modified activated carbons. *Carbon* 35:1339–1348
- Rai HS, Bhattacharyya MS, Singh J, Bansal TK, Vats P, Banerjee UC (2005) Removal of dyes from the effluent of textile and dyestuff manufacturing industry: a review of emerging techniques with reference to biological treatment. *Crit Rev Environ Sci Technol* 35: 219–238
- Regalbuto JR, Robles J (2004) The engineering of Pt/carbon catalyst preparation. University of Illinois, Chicago
- Rodrigues CSD, Madeira LM, Boaventura RAR (2014) Synthetic textile dyeing wastewater treatment by integration of advanced oxidation and biological processes performance analysis with costs reduction. *J Environ Chem Eng* 2:1027–1039
- Royer B, Cardoso NF, Lima EC, Vagheti JCP, Simon NM, Calvete T, Veses RC (2009) Applications of Brazilian pine-fruit shell in natural and carbonized forms as adsorbents to removal of methylene blue from aqueous solutions—kinetic and equilibrium study. *J Hazard Mater* 164:1213–1222
- Ruthven DM (1984) *Principles of adsorption and adsorption processes*. John Wiley & Sons, New York
- Sahu JN, Acharya J, Meikap BC (2010) Optimization of production conditions for activated carbons from tamarind wood by zinc chloride using response surface methodology. *Bioresour Technol* 101:1974–1982
- Saitoh T, Saitoh M, Hattori C, Hiraide M (2014) Rapid removal of cationic dyes from water by co precipitation with aluminum hydroxide and sodium dodecyl sulfate. *J Environ Chem Eng* 2:752–758
- Saygili H, Guzel F (2016) High surface area mesoporous activated carbon from tomato processing solid waste by zinc chloride activation: process optimization, characterization and dyes adsorption. *J Clean Prod* 113:995–1004
- Sing KSW (1989) The use of gas adsorption for the characterization of porous solids. *Colloids Surf* 38:113–124
- Souza TNV, Carvalho SML, Vieira MGA, da Silva MGC, Brasil DSB (2018) Adsorption of basic dyes onto activated carbon: experimental and theoretical investigation of chemical reactivity of basic dyes using DFT-based descriptors. *Appl Surf Sci* 448:662–670
- Sulak MT, Demribas E, Kobya M (2007) Removal of Astrazon Yelooow 7 GL from aqueous solutions by adsorption onto wheat bran. *Bioresour Technol* 98:2590–2598
- Tran HN, You SJ, Chao HP (2017) Activated carbons from golden shower upon different chemical activation methods: synthesis and characterizations. *Adsorpt Sci Technol* 0:1–19
- Vimonses V, Lei S, Jin B, Chow CWK, Saint C (2009) Adsorption of congo red by three Australian kaolins. *Appl Clay Sci* 43:465–472
- Wang XS, Li ZZ, Tao SR (2009) Removal of chromium (VI) from aqueous solution using walnut hull. *J Environ Manag* 90:721–729
- Weber WJ, Morris JC (1963) Kinetics of adsorption on carbon from solution. *J Sanit Eng Div* 89:31–60

- Weber CT, Collazzo GC, Mazutti MA, Foletto EL, Dotto GL (2014) Removal of hazardous pharmaceutical dyes by adsorption onto papaya seeds. *Water Sci Technol* 70:102–107
- Wu JS, Liu CH, Chu KH, Suen SY (2008) Removal of cationic dye methyl violet 2B from water by cation exchange membranes. *J Membr Sci* 309:239–245
- Yakout SM, Daifullah AAM, El-Reefy SA, Ali HF (2013) Surface modification and characterization of a RS activated carbon: density, yield, XRD, ash, and moisture content. *Desalin Water Treat* 53:718–726
- Yeganeh MM, Kaghazchi T, Soleimani M (2006) Effect of raw materials on properties of activated carbons. *Chem Eng Technol* 29:1247–1251
- Zhou L, Jin J, Liu Z, Liang X, Shang C (2011) Adsorption of acid dyes from aqueous solutions by the ethylenediamine-modified magnetic chitosan nanoparticles. *J Hazard Mater* 185:1045–1052